Electron transfer in fast proton-helium collisions

Hong-Keun Kim,[1,*] M. S. Schöffler,[1,2] S. Houamer,[3] O. Chuluunbaatar,[4] J. N. Titze,[1] L. Ph. H. Schmidt,[1] T. Jahnke,[1] H. Schmidt-Böcking,[1] A. Galstyan,[5] Yu. V. Popov,[6] and R. Dörner[1]

[1]*Institut für Kernphysik, University Frankfurt, Max-von-Laue-Strasse 1, D-60438 Frankfurt, Germany*

[2]*Photonics Institute, Technical University Vienna, Gusshausstrasse 27-29, A-1040 Vienna, Austria*

[3]*Laboratoire de Physique Quantique et Systèmes Dynamiques, Département de Physique, Faculté des Sciences, Université Ferhat Abbas, Sétif 19000, Algeria*

[4]*Laboratory of Information Technologies, Joint Institute for Nuclear Research, Dubna, Moscow Region 141980, Russia*

[5]*Faculty of Physics, Moscow State University, Moscow 119991, Russia*

[6]*Nuclear Physics Institute, Moscow State University, Moscow 119991, Russia*

(Received 2 January 2012; published 14 February 2012)

We have measured the electron-transfer process in fast collisions (630–1200 keV/u) of protons with helium, which is dependent on the projectile scattering angle and the final electronic state. The fully differential data accompanied by theoretical second-order perturbation theory allow a detailed insight into the mechanism of electron-transfer processes.

DOI: 10.1103/PhysRevA.85.022707 PACS number(s): 34.70.+e, 34.50.Fa

I. INTRODUCTION

Electron transfer as the source of energy transfer is a hot topic especially in microbiology and also in chemistry and physics. It also attracts quite some interest in astronomy and astrophysics. While in microbiology and chemistry usually the relative velocities between the transfer partners are rather low, the "interstellar" electron transfer happens at MeV or even GeV energies. One might expect that nearly 100 years after the formulation of modern quantum mechanics and perturbation theory, the transfer process, especially in a simple system like $p + \mathrm{He} \rightarrow \mathrm{H}^0 + \mathrm{He}^+$, where just four particles in total are involved, should no longer need to be discussed. A short review of the literature shows, however, that there are many papers published on this or similar collision systems, and many more on electron-transfer processes in collisions in general. But only a tiny fraction of them takes the finally populated electronic states into account: theories usually focus on the ground state (initial and final states), while experiments integrate over all finally populated electronic states. With increasing projectile energy the measurement of the projectile energy loss, which is a key observable in identifying excitation processes, becomes more and more challenging. On the other hand theories get better if the number of relevant interactions is rather low, e.g., at high projectile energies.

Most of theories at high energies are based on different Born approximations: first- and second-order plane wave, distorted wave, time dependent and independent, etc. (see [1] for a recent review). All of them concern an approximation of the four-body wave function with a corresponding boundary condition. No analytical solution of the Schrödinger equation with mutual Coulomb potential between particles is known in this case, and its numerical solution is restricted to relatively low energies. It became clear a long time ago, that first-order Born terms are not able to describe fast-projectile capture processes even at very small scattering angles. In turn, second-order Born terms include summation and integration over the intermediate eigenfunctions of both final fragments. This problem also demands consideration of various approximations and simplifications, the validity of which can be verified only by comparison with experiment. Even within the models, the resulting matrix elements are six- and nine-dimensional integrals with a few highly oscillating integrands, the calculation of which needs special numerical techniques. That is why the theoretical treatment of such "simple" processes is not trivial.

Here we investigate the reaction $p + \mathrm{He} \rightarrow \mathrm{H}^0(n) + \mathrm{He}^+(n')$ at around 1 MeV projectile energies and small (up to 1.5 mrad) hydrogen scattering angles. In the literature two main mechanisms for electron transfer are distinguished: kinematic capture and the Thomas process (see [2,3] for a review). In classical physics the main requirement of electron transfer is that the projectile proton and electron have equal and parallel velocities.

Kinematic capture is a pure quantum-mechanical process, described by Oppenheimer, Brinkman, and Kramers (OBK) [4,5]. It can happen at any relative velocities and angles of the captured electron and projectile proton. The OBK term leads to a main contribution to the single-differential cross section (SDCS) at very small scattering angles around 0.1 mrad.

The Thomas process [6] originates from the classical description by Thomas in 1927, who suggested a double-scattering process leading to electron capture at high impact energies: The projectile scatters at a target electron at a fixed angle of 60°. In the next step, this electron elastically scatters on the target nucleus again at 60°, so finally the electron becomes accelerated from rest to projectile velocity and in the same direction. Alternatively the second scattering process can also occur between two target electrons with a slightly modified collision geometry: 45° instead of the former 60° is necessary. Furthermore, this so called electron-electron Thomas process [7] by definition leads to an additional target excitation, as the second electron gains the same momentum vector as the captured one. Both Thomas processes have a quite rigid collision geometry and therefore a discrete momentum transfer that leads to distinct structures in momentum space.

*kim@atom.uni-frankfurt.de

This fingerprint shows up in the transverse momentum transfer, i.e., the projectile scattering angle, and is 0.45 mrad (e-e) and $\sin(60^\circ) \times m_e/m_P = 0.47$ mrad (N-e), N stands for nucleus. Quantum mechanics and the broad initial or final state of the electron momentum, i.e., the momentum acceptance for the capture process, smear out the δ structure to a broad peak that is centered around the original value. The first observation of the Thomas process in the projectile scattering angle was reported by Horsdal-Pedersen *et al.* [8]. Recent experiments by Fischer and co-workers [9] have validated the velocity dependency and also the enhancement of the cross section around 0.5 mrad [1,10].

Nowadays the experiments measure the projectile and recoiling ion in coincidence and are able to determine in addition to the scattering angle also the overall energy exchange. This Q value (the difference of the binding energies in the initial and final states) is related to the recoil longitudinal momentum $K_{||}$ via the following relation [11,12]:

$$K_{||} = -\frac{Q}{v_p} - \frac{v_p}{2}. \tag{1}$$

From this equation it is obvious that a separation of different electronic states is more difficult for higher projectile velocities and quite easy for low impact velocities, as for example shown in Ref. [13].

In this paper we report differential cross sections for electron transfer in proton-helium collisions at 630, 1000, and 1200 keV/u with sufficient resolution to distinguish final electronic states. We used the cold target recoil ion momentum spectroscopy [14–16] technique and a spectrometer optimized for high momentum resolution. A momentum resolution of 0.04 a.u. was achieved, which is a factor of 4 better than the resolution obtained in the best previous experiment in ion-atom collisions [17].

II. EXPERIMENT

The experiments on electron transfer in proton-helium collisions were conducted at the Institut für Kernphysik, University of Frankfurt. The proton beam was provided from a 2.5 MV Van de Graaff accelerator. A 5 m collimation distance was used to obtain a beam of 0.5×0.5 mm^2 that intersected with the helium target. Shortly before the target a set of electrostatic deflector plates was used to clean the beam from charge-state impurities, originating from electron capture in the beamline. After the beam passed or interacted with the target, a set of electrostatic deflector plates separated the main beam, which was dumped in a Faraday cup, from the charge-exchanged projectiles (H^0). The latter were detected on a 40-mm-diameter time- and position-sensitive multichannel plate (MCP) detector with delay line anode [18,19] and used as the trigger for data acquisition. A supersonic gas jet at room temperature with two stages provided an internal cold and well-localized target beam. With an applied driving pressure of 18 bar, the gas expanded through a 30 μm nozzle, was geometrically collimated 35 mm above the nozzle with a 0.5 mm aperture to a diameter of 1.5 mm and 2×10^{11} helium atoms/cm^2 at the intersection point with the proton beam. Helium ions created by the interaction with the protons perpendicular to the initial beam axis are extracted by applying a weak electrostatic field of 8.96 V/cm. To gain maximum momentum resolution, the spectrometer was built in a time- and space-focusing geometry. Therefore an electrostatic lens in the extraction field focused the 1.5-mm-wide interaction region down to 0.25 mm (see [20] for general information about time and space focusing). Furthermore, a field-free drift tube was added behind the extraction field to compensate the target size in the time-of-flight (TOF) direction. Another time- and position-sensitive MCP detector (80 mm diameter) at the end of the field-free drift tube was used to detect the singly charged He^+ ions. The overall spectrometer length from the interaction point to the detector was 168 cm. This resulted in times of flight of 16 μs for He^+ ions and a 4π solid angle for transverse momenta up to 9 a.u.

As the final state exhibits only two particles, the neutral H^0 and the recoiling He^+ ion, one balances the momentum of the other [21]. Nevertheless, the two particles are measured in coincidence to suppress background and to have a reference signal for the TOF measurement. The momenta shown were deduced from the He^+ ion, as this has by far the better resolution. A rather low count rate of 50 to 500 Hz on the projectile detector and the good spatial separation of target ionization (the main source of random coincidences) and electron transfer on the recoil-ion detector provided a nearly background-free measurement. In Fig. 1(a) the momenta on the plane of the recoil detector are shown for a projectile energy of 1200 keV/u. The vertical lines represent the electron transfer marked as "single-capture"; the round blob is target (single) ionization. The remaining broadly distributed events for small $p_{y,\mathrm{jet}}$ stem from residual gas ionization. According to Eq. (1) the longitudinal momentum $p_{||}$ in a capture process can be calculated for a given projectile velocity $\vec{v}_p$ and Q value. Since different states in the electronic excitation of the single-capture process exhibit different Q values, the separation of several states can be observed in Fig. 1(b). Here the transverse momentum of the He^+ recoil ions p_θ which corresponds to the scattering angle of the projectiles is plotted versus the longitudinal momentum for $-3.6 < p_{||} < -3.0$ a.u. The electronic ground state of the ion $He^+(n' = 1)$ ($p_{||} < -3.3$ a.u.) was clearly separated from the excited states $He^+(n' \geqslant 2)$ ($p_{||} > -3.3$ a.u.). Additionally the higher excited states of H^0 ($n \geqslant 2$) could be resolved from the H^0 ($n = 1$) ground state. The momentum resolution achieved in the longitudinal direction was 0.04 a.u. for all three projectile energies [see Figs. 2(a)–2(c) for $E_{\mathrm{proj}} = 630$, 1000, and 1200 keV/u, respectively].

III. THEORY

A. General formulation

The amplitude of the charge-transfer reaction under consideration takes the form

$$T_{fi} = \sqrt{2}\langle \Psi_f^-(\vec{R},\vec{\rho},\vec{r}_2)|V_{p1} + V_{p2} + V_{pN}|\Psi_i^+(\vec{r}_p,\vec{r}_1,\vec{r}_2)\rangle. \tag{2}$$

In Eq. (2) $\vec{r}_p$ is the proton coordinate, $\vec{r}_1$ the coordinate of the electron adjoint to the proton in the final state, and $\vec{r}_2$ the same for the He^+ residual ion. The symmetrization is already done

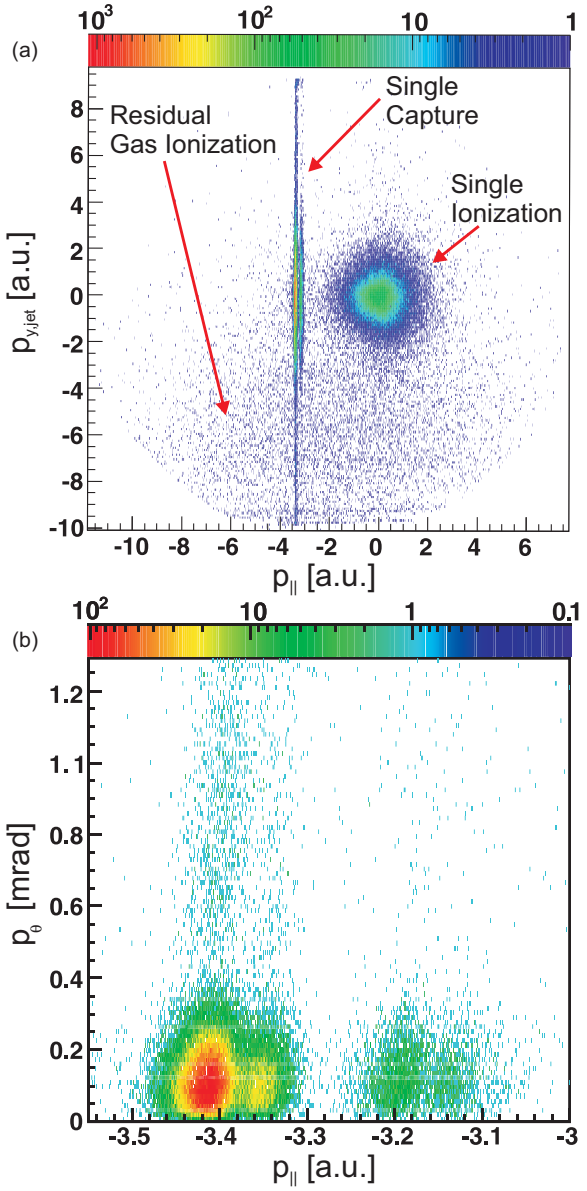

FIG. 1. (Color online) (a) The momenta in the plane of the recoil detector for a projectile energy of 1200 keV/u. The vertical lines represent the electron transfer marked as single-capture; the round blob is the target single ionization. The remaining broadly distributed events for small $p_{y,\mathrm{jet}}$ stem from residual gas ionization. (b) The transverse momentum of the He^+ recoil ions p_θ vs the longitudinal momentum $p_{||}$ for the same projectile energy as in (a). The events are distributed around $p_{||} = -3.42$ a.u., -3.35 a.u., -3.20 a.u., and -3.12 a.u. (Gaussian fit analysis), and are attributed to the single-capture ground state, projectile excitation, target excitation, and simultaneous projectile and target excitation, respectively.

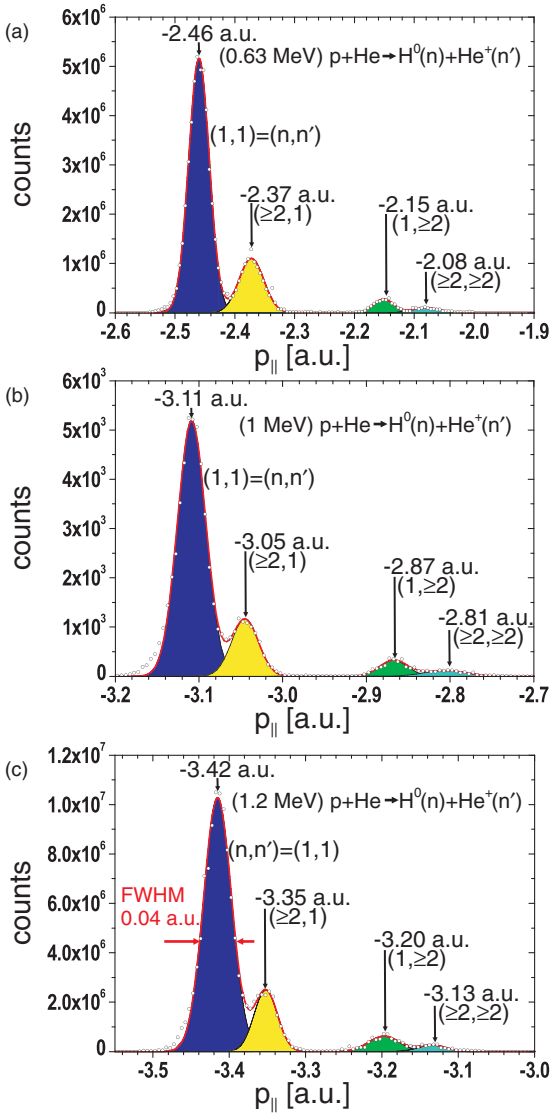

FIG. 2. (Color online) The longitudinal momentum distribution of the recoil ion (He^+) for the projectile energies (a) 630, (b) 1000, and (c) 1200 keV. At least four peaks can be resolved from left to right: the electronic ground state of the projectile $H^0(n)$ and target $He^+(n')$ ($n = 1$, $n' = 1$), projectile excitation and target ground state ($n \geqslant 2$, $n' = 1$), projectile ground state and target excitation ($n = 1$, $n \geqslant 2$), and simultaneous projectile and target excitation ($n \geqslant 2$, $n' \geqslant 2$).

in Eq. (2). The other definitions are as follows:

$$\vec{R} = \frac{m\vec{r}_p + \vec{r}_1}{m+1}, \quad \vec{\rho} = \vec{r}_p - \vec{r}_1,$$

or

$$\vec{r}_p = \vec{R} + \frac{1}{m+1}\vec{\rho}, \quad \vec{r}_1 = \vec{R} - \frac{m}{m+1}\vec{\rho} \approx \vec{R} - \vec{\rho}.$$

We also note $\vec{p}_p \cdot \vec{r}_p \approx \vec{p}_p \cdot \vec{R} + \vec{v}_p \cdot \vec{\rho}$. For very small scattering angles we suppose that the nucleus is immovable, i.e., $r_N = 0$. Here $m = 1836.15$ a.u. is the proton mass, and $\mu = m/(m+1) \approx 1$ is the reduced mass.

All six Coulomb potentials between particles now appear as

$$V_{p1} = -\frac{1}{|\vec{r}_p - \vec{r}_1|} = -\frac{1}{\rho}; \quad V_{p2} = -\frac{1}{|\vec{r}_p - \vec{r}_2|} \approx -\frac{1}{|\vec{R} - \vec{r}_2|};$$

$$V_{pN} = \frac{2}{|\vec{r}_p - \vec{r}_N|} \approx \frac{2}{R}; \quad V_{N2} = -\frac{2}{|\vec{r}_N - \vec{r}_2|} \approx -\frac{2}{r_2};$$

$$V_{N1} = -\frac{2}{|\vec{r}_N - \vec{r}_1|} \approx -\frac{2}{|\vec{R} - \vec{\rho}|};$$
$$V_{12} = \frac{1}{|\vec{r}_1 - \vec{r}_2|} \approx \frac{1}{|\vec{R} - \vec{\rho} - \vec{r}_2|}.$$

We write the initial state in the form

$$\Psi_i^+(\vec{r}_p,\vec{r}_1,\vec{r}_2) = e^{i\vec{p}_p\cdot\vec{r}_p}\Phi_0(\vec{r}_1,\vec{r}_2) \approx e^{i\vec{p}_p\cdot\vec{R}}\, e^{i\vec{v}_p\cdot\vec{\rho}}\Phi_0(\vec{R} - \vec{\rho},\vec{r}_2). \quad (3)$$

The final wave function satisfies the equation

$$\left[\frac{1}{2(m+1)}\Delta_R + \left(\frac{1}{2\mu}\Delta_\rho - V_{p1}\right) + \left(\frac{1}{2}\Delta_2 - V_{N2}\right) + E\right] \times \Psi_f^-(\vec{R},\vec{\rho},\vec{r}_2) = [V_{p2} + V_{pN} + V_{N1} + V_{12}]\Psi_f^-(\vec{R},\vec{\rho},\vec{r}_2) \quad (4)$$

with boundary conditions

$$\Psi_f^-(\vec{R},\vec{\rho},\vec{r}_2)_{R\to\infty} \sim e^{i\vec{p}_H\cdot\vec{R}}\varphi_0(\rho)\phi_\alpha^-(\vec{r}_2) \quad (5)$$

where $\phi_\alpha^-(\vec{r}_2)$ is in the general case the eigenfunction of the helium ion. We denote the transferred momentum as $\vec{q} = \vec{p}_H - \vec{p}_p$. In Eq. (4) the total energy

$$E = \frac{p_p^2}{2m} + \varepsilon_0^{He} = \frac{p_H^2}{2(m+1)} + \varepsilon_0^H + \varepsilon_\alpha^{He^+}. \quad (6)$$

For charge-transfer (CT) reactions we set $\varepsilon_\alpha^{He^+} = \varepsilon_0^{He^+} = -2$; for transfer-ionization reactions $\varepsilon_\alpha^{He^+} = k^2/2$. Choosing the vector $\vec{v}_p$ as the z axis, it follows from Eq. (6) that $q_z = v_p/2 + Q/v_p$. In the case of the CT reaction $Q = \varepsilon_0^{He} - \varepsilon_0^H - \varepsilon_0^{He^+} \approx -0.403$ [see (1)] . The perpendicular component of the vector $\vec{q}$ is $q_\perp \approx m v_p \theta_p$.

Because the proton is a heavy fast particle, we look for the solution in the form (the so-called paraxial approximation)

$$\Psi_f^-(\vec{R},\vec{\rho},\vec{r}_2) = e^{i\vec{p}_H\cdot\vec{R}}\,\Phi_f^-(\vec{R},\vec{\rho},\vec{r}_2). \quad (7)$$

Inserting (7) into (4) and taking into account (6), we obtain

$$\left[\left(\frac{1}{2(m+1)}\Delta_R + i\vec{v}_p\cdot\vec{\nabla}_R\right) + \left(\frac{1}{2\mu}\Delta_\rho + \varepsilon_0^H - V_{p1}\right) + \left(\frac{1}{2}\Delta_2 + E_\alpha^{He^+} - V_{N2}\right)\right]\Phi_f^-(\vec{R},\vec{\rho},\vec{r}_2) = [V_{p2} + V_{pN} + V_{N1} + V_{12}]\,\Phi_f^-(\vec{R},\vec{\rho},\vec{r}_2). \quad (8)$$

Now as in the eikonal approximation we neglect $\Delta_R/2(m+1)$ in Eq. (8). Here we have a rather strong argument for doing this as the proton mass is in the denominator. In the residual equation we can replace $z_R = v_p t$ and obtain from (8)

$$i\frac{\partial}{\partial t}\Phi_f^-(\vec{R}_\perp,\vec{\rho},\vec{r}_2;t) = \left[-\left(\frac{1}{2\mu}\Delta_\rho + \varepsilon_0^H - V_{p1}\right) - \left(\frac{1}{2}\Delta_2 + E_\alpha^{He^+} - V_{N2}\right) + V_{p2}(t) + V_{pN}(t) + V_{N1}(t) + V_{12}(t)\right]\Phi_f^-(\vec{R}_\perp,\vec{\rho},\vec{r}_2;t). \quad (9)$$

Now $\vec{R} = (\vec{R}_\perp, v_p t)$. The initial condition of this "time-dependent" equation takes the form

$$\Phi_f^-(\vec{R}_\perp,\vec{\rho},\vec{r}_2;t)_{t\to\infty} = \varphi_0(\rho)\phi_\alpha^-(\vec{r}_2). \quad (10)$$

Equation (9) recalls the widely known time-dependent approach when the proton is considered from the beginning like a classical particle (the source of the external time-dependent Coulomb field), but here this equation appears on the basis of a pure quantum approach and is applied only to the calculation of the final wave function.

The matrix element (2) reads like a nine-dimensional (9D) integral

$$T_{fi} = \sqrt{2}\int d^3R e^{-i\vec{R}\cdot\vec{q}}\int d^3\rho e^{i\vec{\rho}\cdot\vec{v}_p}\int d^3r_2\Phi_f^{-*}(\vec{R},\vec{\rho},\vec{r}_2) \times\left[-\frac{1}{\rho} - \frac{1}{|\vec{R} - \vec{r}_2|} + \frac{2}{R}\right]\Phi_0(\vec{R} - \vec{\rho},\vec{r}_2). \quad (11)$$

The single-differential cross section for charge-transfer reactions takes the form

$$\frac{d\sigma}{d\theta_p} = \frac{m^2\theta_p}{(2\pi)}|T_{fi}|^2. \quad (12)$$

B. Closure approximation: Distorted-wave Born approximation

We denote the operator $\hat{\mathcal{H}}_0 = (\hat{H}_0^H - \varepsilon_0^H) + (\hat{H}_0^{He^+} - \varepsilon_0^{He^+})$. The formal solution of Eq. (9) can be written as

$$|\Phi_f^-(t)\rangle = e^{-i\hat{\mathcal{H}}_0 t}|C(t)\rangle,$$

and

$$i\frac{\partial}{\partial t}C(\vec{R}(t),\vec{\rho},\vec{r}_2;t) = e^{i\hat{\mathcal{H}}_0 t} \times\left[\frac{2}{R(t)} - \frac{2}{|\vec{R}(t) - \vec{\rho}|} - \frac{1}{|\vec{R}(t) - \vec{r}_2|} + \frac{1}{|\vec{R}(t) - \vec{\rho} - \vec{r}_2|}\right] \times e^{-i\hat{\mathcal{H}}_0 t}C(R(t),\vec{\rho},\vec{r}_2;t), \quad (13)$$

with $C(t)_{t\to\infty} = \varphi_0(\rho)\phi_\alpha^-(\vec{r}_2)$.

Now we apply the closure approximation to (13), replacing $\hat{\mathcal{H}}_0 \to \bar{E} > 0$. In this case Eq. (13) can be easily integrated, and we obtain

$$C(\vec{R}(t),\vec{\rho},\vec{r}_2)_{clos} = \exp\left(\frac{i}{v_p}f(t)\right)\,\varphi_0(\rho)\phi_\alpha^-(\vec{r}_2)$$

and

$$f(t) = \ln\left[\frac{\{v_p|\vec{R}(t) - \vec{\rho}| + \vec{v}_p\cdot[\vec{R}(t) - \vec{\rho}]\}^2\,\{v_p|\vec{R}(t) - \vec{r}_2| + \vec{v}_p\cdot[\vec{R}(t) - \vec{r}_2]\}}{[v_p R(t) + \vec{v}_p\cdot\vec{R}(t)]^2\,\{v_p|\vec{R}(t) - \vec{\rho} - \vec{r}_2| + \vec{v}_p\cdot[\vec{R}(t) - \vec{\rho} - \vec{r}_2]\}}\right]. \quad (14)$$

In the closure approximation the solution of Eq. (9) takes the form

$$|\Phi_f^-(t)\rangle = e^{-i\hat{\mathcal{H}}_0 t}|C(t)\rangle = e^{-i\hat{\mathcal{H}}_0 t}\, e^{[(i/v_p)f(t)]} e^{i\hat{\mathcal{H}}_0 t}|C(\infty)\rangle \approx e^{[(i/v_p)f(t)]}|C(\infty)\rangle. \quad (15)$$

The matrix element (11) reads now (we returned to $z_R = v_p t$)

$$T_{fi} \approx \sqrt{2}\int d^3R e^{-i\vec{R}\cdot\vec{q}} \int d^3\rho e^{i\vec{\rho}\cdot\vec{v}_p}\, \varphi_0(\rho) \int d^3r_2 \phi_\alpha^{-*}(\vec{r}_2) \times e^{[-(i/v_p)f(\vec{R},\vec{\rho},\vec{r}_2)]}\left[-\frac{1}{\rho} - \frac{1}{|\vec{R}-\vec{r}_2|} + \frac{2}{R}\right] \times \Phi_0(\vec{R}-\vec{\rho},\vec{r}_2). \quad (16)$$

It is interesting to note that the closure approximation in this approach does not contain a fitting parameter, which is a typical feature of the second-order Born theory.

If we neglect the distorting term $\exp[-(i/v_p)f(\vec{R},\vec{\rho},\vec{r}_2)]$ in Eq. (16), i.e., replace it by 1, the plane-wave first-order Born approximation (PWFBA) follows. The corresponding 9D integral can be reduced now to 3D [for details, see [22]; also Eq. (20) below].

We can slightly simplify the 9D integral in Eq. (16) in the case of the CT reaction $[\phi_\alpha^-(\vec{r}_2) \equiv \phi_0(\vec{r}_2)]$. First, we consider the simplest helium ground-state wave function; it is the Hylleraas one

$$\Phi_0(\vec{r}_1,\vec{r}_2) \approx \Phi_{\rm Hy}(r_1)\Phi_{\rm Hy}(r_2), \qquad \Phi_{\rm Hy}(r) = \sqrt{\frac{Z^3}{\pi}}e^{-Zr}, \quad Z = 27/16. \quad (17)$$

It was noted in our previous investigation that any helium trial wave function gives the same angular distribution in the vicinity of the main peak (see [22], Fig. 3) for CT reactions.

Second, at large v_p, q, only small values of $(\rho, R) \sim 1/v_p$ contribute to the integral (16) because of the highly oscillating integrands, in contrast to r_2. Thus, one easily sees that if $\rho, R \ll r_2$, we can consider a model where the ion He^+ stays nonperturbed during the time of interaction, which is about $t_{\rm int} \approx 2r_{\rm He}/v_p^2$. In this particular case,

$$T_{fi} = \sqrt{2}\int d^3R e^{-i\vec{R}\cdot\vec{q}} \int d^3\rho e^{i\vec{\rho}\cdot\vec{v}_p}\, \varphi_0(\rho)\, e^{[-(2i/v_p)g(\vec{R},\vec{\rho})]} \times \left[-\frac{a}{\rho} - b + \frac{2a}{R}\right]\Phi_{\rm Hy}(\vec{R}-\vec{\rho}) \quad (18)$$

with

$$a = \langle\phi_0|\Phi_{\rm Hy}\rangle = \frac{8(2Z)^{3/2}}{(Z+2)^3}, \quad b = \langle\phi_0|\frac{1}{r_2}|\Phi_{\rm Hy}\rangle = \frac{4(2Z)^{3/2}}{(Z+2)^2},$$

and

$$g(\vec{R},\vec{\rho}) = \ln\left[\frac{[v_p|\vec{R}-\vec{\rho}| + \vec{v}_p\cdot(\vec{R}-\vec{\rho})]}{[v_pR + \vec{v}_p\cdot\vec{R}]}\right].$$

Results of calculations of the 6D integral (18) (with and without g) are presented in Figs. 9–11.

C. Closure approximation: Plane-wave second-order Born approximation

The plane-wave second-order Born approximation (PWSBA) obviously follows from Eq. (9). To write suitable formulas we define $\varphi_\alpha(\vec{\rho})$ as a spectral state of hydrogen and $\phi_\beta(\vec{r}_2)$ as a spectral state of the He^+ ion. A tilde indicates these functions in momentum space. We also define the matrix elements

$$F_\beta(\vec{\xi},\vec{\eta}) = \int d^3r_1 d^3r_2 e^{-i\vec{\xi}\cdot\vec{r}_1} e^{-i\vec{\eta}\cdot\vec{r}_2}\phi_\beta^*(\vec{r}_2)\Phi_0(\vec{r}_1,\vec{r}_2) \quad (19)$$

and partial amplitudes

$$T_{\alpha\beta}(\vec{q}-\vec{x}) = -4\pi\sqrt{2}\int \frac{d^3s}{(2\pi)^3}\frac{\tilde{\varphi}_\alpha^*(\vec{s})}{(\vec{v}_p - \vec{q} + \vec{x} - \vec{s})^2}[F_\beta(\vec{q}-\vec{x},0) + F_\beta(\vec{v}_p - \vec{s}, -\vec{v}_p + \vec{q} - \vec{x} + \vec{s}) - 2F_\beta(\vec{v}_p - \vec{s},0)]. \quad (20)$$

In these definitions $T_{fi}^{\rm FBA} \equiv T_{00}(\vec{q})$.

We would like to make a few clarifications here. The PWFBA consists of three terms. The first one is just the plane-wave OBK term mentioned in the Introduction. The third one includes the proton-nucleus interaction. Both these terms describe the shake-off process in the target. The second term in Eq. (20) describes the sequential interaction of the proton with both target electrons, but it is still a first-order Born term, because only one actual scattering intermediate interaction is involved.

We omit intermediate computations and write the PWSBA amplitude as $T_{fi}^{\rm SBA} = (B_1 + B_2 + B_3 + B_4)$. The term B_1 is associated with the interaction V_{p2} in the final state and is equal to

$$B_1 = -\sum_\beta \int \frac{d^3x}{(2\pi)^3}\frac{4\pi}{x^2}\frac{\langle\phi_0|e^{-i\vec{x}\cdot\vec{r}_2}|\phi_\beta\rangle}{\vec{v}_p\cdot\vec{x} + \left(\varepsilon_0^{\rm He^+} - \varepsilon_\beta^{\rm He^+}\right) + i0} \times T_{0\beta}(\vec{q}-\vec{x}).$$

It includes all intermediate excitations of the helium ion. The term B_2 is associated with the interaction V_{pN} in the final state and is equal to

$$B_2 = 2\int \frac{d^3x}{(2\pi)^3}\frac{4\pi}{x^2}\frac{1}{\vec{v}_p\cdot\vec{x} + i0}\, T_{00}(\vec{q}-\vec{x}).$$

The term B_3 is associated with the interaction V_{N1} in the final state:

$$B_3 = -2\sum_\alpha \int \frac{d^3x}{(2\pi)^3}\frac{4\pi}{x^2}\frac{\langle\varphi_0|e^{-i\vec{x}\cdot\vec{\rho}}|\varphi_\alpha\rangle}{\vec{v}_p\cdot\vec{x} + \left(\varepsilon_0^{\rm H} - \varepsilon_\alpha^{\rm H}\right) + i0} \times T_{\alpha 0}(\vec{q}-\vec{x}),$$

and includes intermediate excitations of the hydrogen atom. Finally, the term B_4 is associated with the interaction V_{12} in the final state and is equal to

$$B_4 = \sum_{\alpha,\beta}\int \frac{d^3x}{(2\pi)^3}\frac{4\pi}{x^2}\frac{\langle\varphi_0|e^{-i\vec{x}\cdot\vec{\rho}}|\varphi_\alpha\rangle\langle\phi_0|e^{-i\vec{x}\cdot\vec{r}_2}|\phi_\beta\rangle}{\vec{v}_p\cdot\vec{x} + \left(\varepsilon_0^{\rm H} - \varepsilon_\alpha^{\rm H}\right) + \left(\varepsilon_0^{\rm He^+} - \varepsilon_\beta^{\rm He^+}\right) + i0} T_{\alpha\beta}(\vec{q}-\vec{x}).$$

All intermediate excitations of both helium ion and hydrogen atom are included here. We have to note that the sums $(B_2 + B_3)$ and $(B_1 + B_4)$ compose nondivergent integrals at $x \sim 0$.

Finally, $T_{fi} \approx T_{fi}^{\mathrm{FBA}} + T_{fi}^{\mathrm{SBA}}$.

The PWSBA amplitude can be presented in the closure approximation:

$$T_{fi}^{\mathrm{SBA}} \approx \frac{1}{2\pi^2} \int \frac{d^3x}{x^2} \frac{\{[P_1(\vec{x}) + P_4(\vec{x})] + [P_2(\vec{x}) + P_3(\vec{x})]\}}{\vec{v}_p \cdot \vec{x} - \bar{E} + i0}. \tag{21}$$

Here we again replace the whole spectrum of the operator $\hat{\mathcal{H}}_0$ by an averaged energy $\bar{E} > 0$. In Eq. (21)

$$P_1(\vec{x}) = 4\pi\sqrt{2} \int \frac{d^3s}{(2\pi)^3} \frac{\tilde{\varphi}_0^*(s)}{(\vec{v}_p - \vec{q} + \vec{x} - \vec{s})^2} [F_0(\vec{q} - \vec{x}, \vec{x}) + F_0(\vec{v}_p - \vec{s}, -\vec{v}_p + \vec{q} + \vec{s}) - 2F_0(\vec{v}_p - \vec{s}, \vec{x})];$$

$$P_2(\vec{x}) = -8\pi\sqrt{2} \int \frac{d^3s}{(2\pi)^3} \frac{\tilde{\varphi}_0^*(s)}{(\vec{v}_p - \vec{q} + \vec{x} - \vec{s})^2} [F_0(\vec{q} - \vec{x}, 0) + F_0(\vec{v}_p - \vec{s}, -\vec{v}_p + \vec{q} - \vec{x} + \vec{s}) - 2F_0(\vec{v}_p - \vec{s}, 0)];$$

$$P_3(\vec{x}) = 8\pi\sqrt{2} \int \frac{d^3s}{(2\pi)^3} \frac{\tilde{\varphi}_0^*(s)}{(\vec{v}_p - \vec{q} - \vec{s})^2} [F_0(\vec{q} - \vec{x}, 0) + F_0(\vec{v}_p - \vec{s} - \vec{x}, -\vec{v}_p + \vec{q} + \vec{s}) - 2F_0(\vec{v}_p - \vec{s} - \vec{x}, 0)];$$

$$P_4(\vec{x}) = -4\pi\sqrt{2} \int \frac{d^3s}{(2\pi)^3} \frac{\tilde{\varphi}_0^*(s)}{(\vec{v}_p - \vec{q} - \vec{s})^2} [F_0(\vec{q} - \vec{x}, \vec{x}) + F_0(\vec{v}_p - \vec{s} - \vec{x}, -\vec{v}_p + \vec{q} + \vec{s} + \vec{x}) - 2F_0(\vec{v}_p - \vec{s} - \vec{x}, \vec{x})].$$

The results of calculations of the 6D integrals in Eq. (21) are presented in Figs. 3–5. The method of Laplace transformation (see [23] and Appendixes there) was used for the calculations.

IV. RESULTS AND DISCUSSION

With very good experimental momentum resolution we were able to separate the different excitation processes that can accompany electron transfer, encoded in the longitudinal momentum. From the data and multiple Gaussian fits shown in Fig. 2 we extracted the branching ratios, shown in Table I. The general trend of decreasing excitation with increasing projectile velocity follows the trend of earlier state-selective measurements [24]. Furthermore it agrees well with the intuitive picture that additional interactions become more unlikely at higher projectile velocities.

The theory of capture processes and the main approximations were presented in the review paper of Belkić *et al.* [25] more than 30 years ago, and this paper is still relevant in spite of numerous modifications and improvements given later. Three main theoretical options are available for fast projectile particles: the time-dependent approach, the Born-Faddeev series, and the plane-wave Born series. All of them are connected, if the fast particle is not considered as the classical source of the external time-dependent field. The Born-Faddeev series immediately leads to distorted-wave considerations because the two-body potential which appears in the diagrams of the plane-wave Born series is replaced by the two-body off-shell amplitude. To our knowledge, Alston was the first who used this approach in numerical calculations (see, for example, [23] and references within).

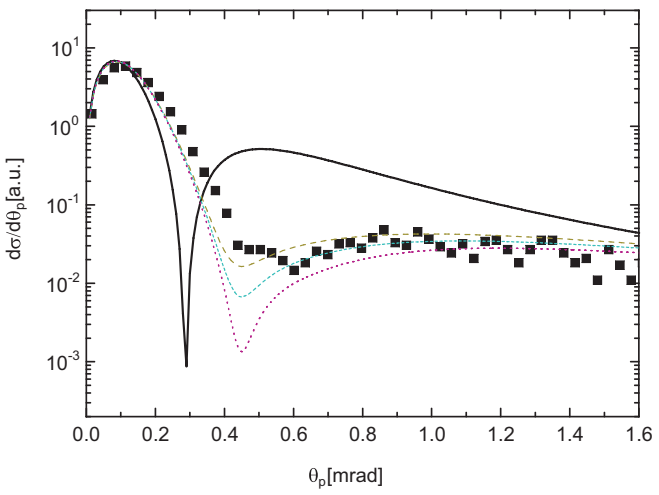

FIG. 3. (Color online) SDCS versus the scattering angle of the final fast hydrogen atom. The projectile proton energy is $E_p =$ 630 keV. Solid line, the PWFBA with Eq. (20); broken lines, the PWSBA with Eq. (21) (long-dashed line, $\bar{E} = 0.1$, short -dashed line, $\bar{E} = 0.5$, dotted line, $\bar{E} = 1$; the tendency is clear). Both hydrogen and the final helium ion are supposed to be in their ground states. The experiment is normalized to the maximum of the PWFBA model.

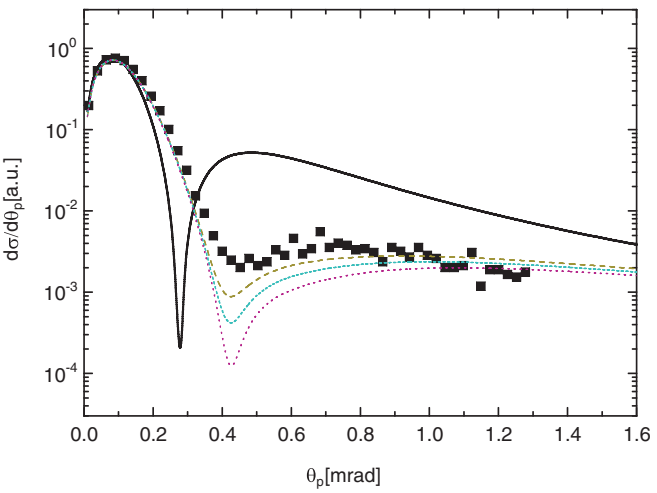

FIG. 4. (Color online) As Fig. 3, but $E_p = 1000$ keV.

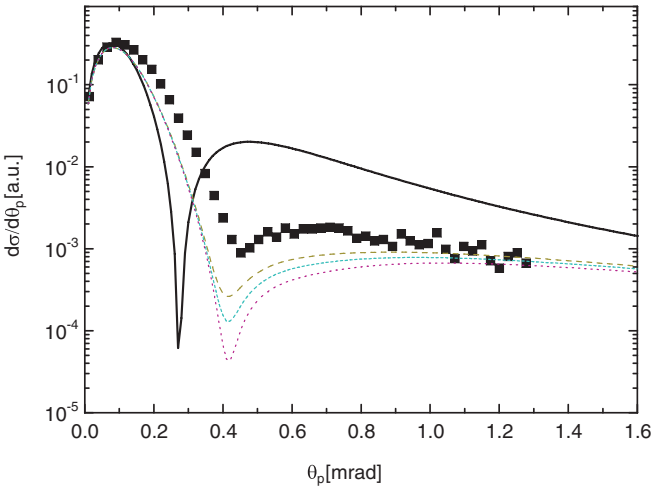

FIG. 5. (Color online) As Fig. 3, but $E_p = 1200$ keV.

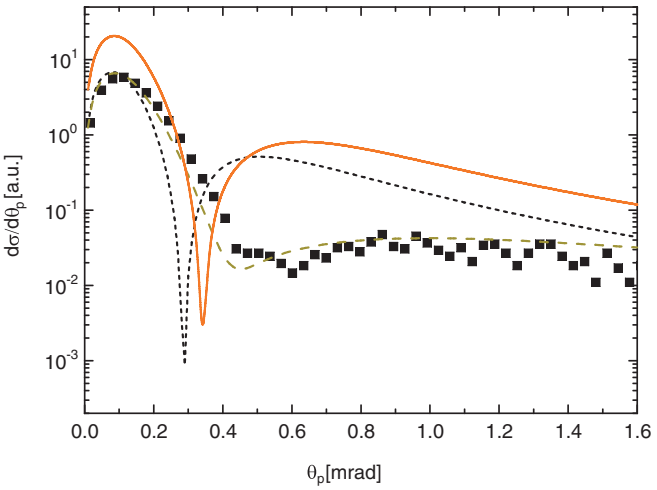

FIG. 6. (Color online) SDCS versus the scattering angle of the final fast hydrogen atom. The projectile proton energy is $E_p = 630$ keV (same data as in Fig. 3). Solid line, the Thomas peak contribution only with the term $B3$; dotted line, the PWFBA; dashed line, the PWSBA with $\bar{E} = 0.1$. Both hydrogen and the final helium ion are supposed to be in their ground states. The experiment is normalized to the maximum of the PWFBA model.

The distorted-wave approach leads to many speculations and is mainly based on asymptotic considerations, while the capture happens inside the target, i.e., large impact parameters do not play any role [see (11)]. One can easily see from (13) and (15) that logarithmic phases appear in Eq. (16), as is typical for old theories, if we neglect any intermediate quantum excitations of colliding components. In this respect, plane-wave theories provide the most transparent physics.

It is quite clear now that the theoretical treatment of high-energy capture processes is much more complicated than that of direct scattering. As in electron momentum spectroscopy (EMS) [26,27], the fast capture processes can be attributed to scattering processes with two fast particles in the final state (see also the review paper [28]). However, in contrast to EMS, the PWFBA does not reproduce the experimental SDCSs. Only the OBK term corresponds closely to the EMS amplitude, but here the term which describes p-N interaction plays a crucial role.

One can see in Figs. 3–5 that the experimental angular distribution exhibits two well-pronounced domains: a sharp peak at about $\theta_p \sim 0.1$ mrad and a rather flat structure above 0.4 mrad. The PWFBA result (solid line) is similar to this structure, but the main peak is much too sharp, and the tail after the minimum is about an order of magnitude bigger. It is interesting to note here once more that the shape and absolute value of the PWFBA theoretical curve do not depend much on the correlation structure of the trial helium ground-state wave function and are defined mainly by its $1s^2$ part. On the basis of this last observation the total cross section (TCS) of the reaction considered here was calculated with the PWFBA, and the result above $E_p = 500$ keV unexpectedly gave rather good coincidence with the experiment [29]. The reason is quite clear; it is because the main peak is sharp, and the angular region 0–0.2 mrad gives the principal contribution to the TCS. That is why we can normalize the corresponding experiment to the peak value of the PWFBA distribution, because in such a way we normalize it to the TCS.

The plane-wave OBK term reproduces much better the shape of the main peak, but it is about three times higher than the PWFBA peak, and the TCS calculated with only the OBK term noticeably exceeds the experimental value. And of

TABLE I. Experimental branching ratios for the electronic states of the single-capture process $[p + \mathrm{He} \rightarrow \mathrm{H}^0(n) + \mathrm{He}^+(n')]$ for projectile energies of 630, 1000, and 1200 keV/u. $n = 1, n' = 1$: electron transfer without excitation; $n \geqslant 2$, $n' = 1$: electron transfer into an excited state of the projectile; $n = 1$, $n' \geqslant 2$: electron transfer with additional target excitation; $n \geqslant 2$, $n' \geqslant 2$: electron transfer with target and projectile excitation. The errors are statistical ones.

	630 keV/u	1000 keV/u	1200 keV/u
$n = 1, n' = 1$	$(74.9 \pm 0.1)\%$	$(76.5 \pm 0.2)\%$	$(77.2 \pm 0.2)\%$
$n \geqslant 2, n' = 1$	$(19.2 \pm 0.1)\%$	$(16.3 \pm 0.2)\%$	$(15.6 \pm 0.2)\%$
$n = 1, n' \geqslant 2$	$(3.9 \pm 0.2)\%$	$(4.7 \pm 0.4)\%$	$(5.2 \pm 0.3)\%$
$n \geqslant 2, n' \geqslant 2$	$(2.0 \pm 0.2)\%$	$(2.5 \pm 0.4)\%$	$(2.0 \pm 0.3)\%$

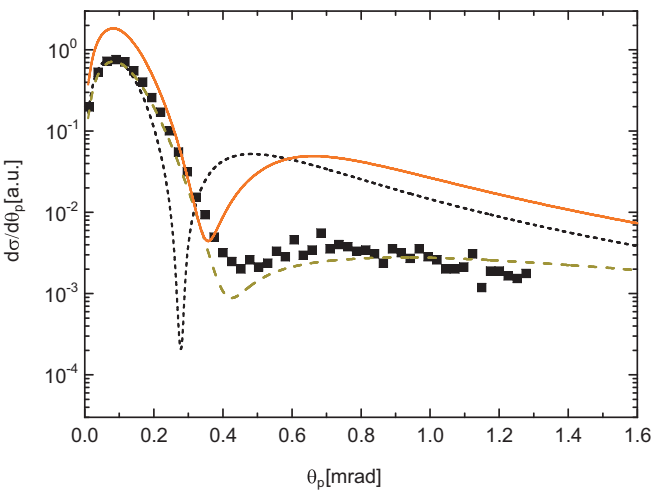

FIG. 7. (Color online) As Fig. 6, but $E_p = 1000$ keV (same data as in Fig. 4).

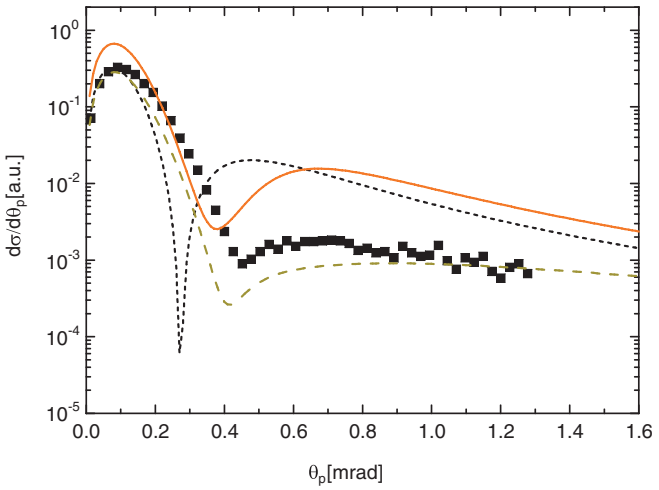

FIG. 8. (Color online) As Fig. 6, but $E_p = 1200$ keV (same data as in Fig. 5).

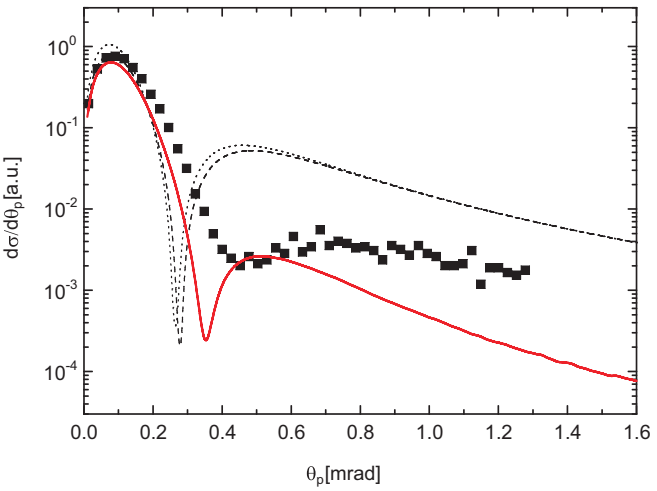

FIG. 10. (Color online) As Fig. 9, but $E_p = 1000$ keV (same data as in Fig. 4).

course the OBK term exhibits no plateau. Consequently, the $p-N$ interaction plays a very important role, as was discussed earlier.

If the PWFBA (mainly the OBK term + p-N) reproduces the domain of kinematic capture ($\theta_p \sim 0.1$ mrad), the recollision processes must play an important role in the region of the plateau and also increase the width of the main peak. Let us analyze more carefully the role of the p-N term. The fast projectile proton meets the nucleus and is slightly deflected from its straight path. The scattering angle depends on the impact parameter and can be easily calculated from classical considerations. Then this proton captures the electron directly by means of the secondary OBK mechanism, but now the momentum transfer is slightly shifted compare to pure OBK capture. The sum of these two amplitudes allows the peak width to be enlarged up to the experimental value ($\theta_p \lesssim 0.4$ mrad) without any noticeable change in its height, but this mechanism does not explain the plateau.

The PWSBA terms contain summation and integration over the intermediate spectra of the hydrogen atom and He^+ ion (terms $B1$–$B4$). This is an impossibly complicated task even for supercomputers, and we have to make further approximations. One of them is the so-called closure approximation, introduced many years ago in nuclear physics. We suppose that in fast collisions all the principal intermediate states are excited with equal probability, which allows us to replace their eigenenergies by an averaged energy, which plays the role of a fitting parameter. These considerations give more or less reasonable results in many cases of fast scattering processes. The results of such calculations with the wave function (17) are presented in Figs. 3–5 (dashed lines). We actually see that the SBA theory results move toward the experimental values, expanding the main peak without changing its height and approaching the plateau from below. But some details cannot be described satisfactorily. The strangest observation is that the

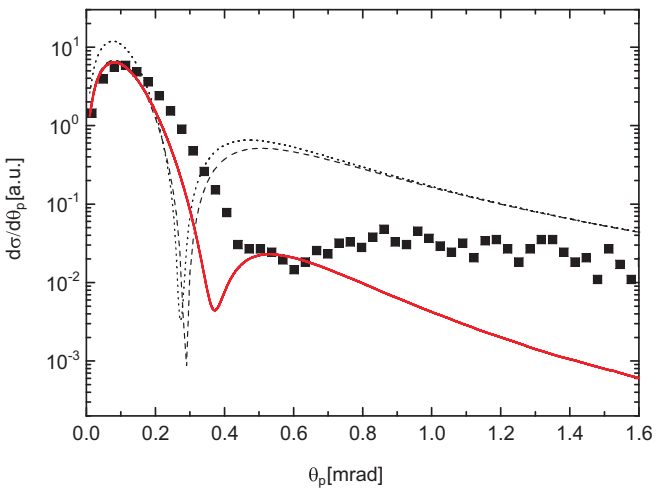

FIG. 9. (Color online) SDCS versus the scattering angle of the final fast hydrogen atom. The projectile proton energy is $E_p = 630$ keV (same data as in Fig. 3). Solid line, the DWBA with Eq. (18); dashed line, the PWFBA with Eq. (20); dotted line, the modified PWFBA with Eq. (18) where $g = 0$. Both hydrogen and the final helium ion are supposed to be in their ground states. The experiment is normalized to the maximum of the PWFBA model.

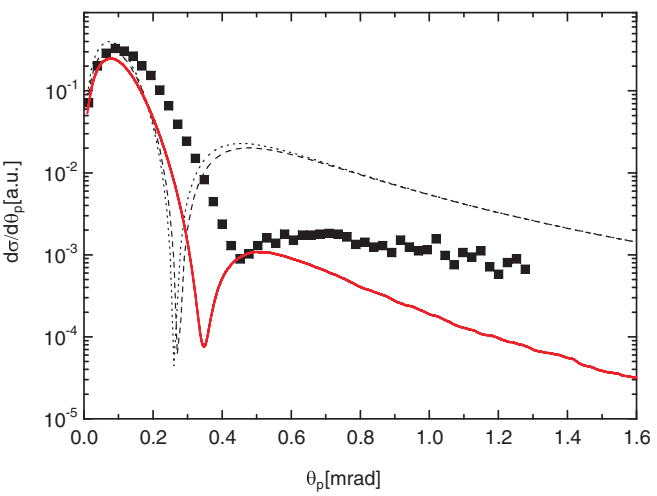

FIG. 11. (Color online) As Fig. 9, but $E_p = 1200$ keV (same data as in Fig. 5).

best fit is reached for $\bar{E} \sim 0$. This means that the "averaged energy" is close to the ground-state intermediate energies of the hydrogen atom and helium ion, i.e., they essentially are not excited in the intermediate state.

This conclusion is in serious contradiction with the proposal that the Thomas mechanism plays a leading role in formation of the plateau ($\theta_p \gtrsim 0.4$ mrad), where the continuum part of the hydrogen spectrum mainly contributes (the term $B3$). Here for the estimations we set $\varphi_\alpha = \exp(i\vec{p}\cdot\vec{\rho})$, i.e., a plane wave, $\varepsilon_\alpha^{\mathrm{H}} = p^2/2$, and the summation is replaced by integration, $d^3p/(2\pi)^3$. The results of the calculations are presented in Figs. 6–8. The tendency to approach the experimental results is seen, but for the proton energies under consideration the results of the calculations are rather far from the experimental values. Perhaps taking into account Coulomb waves instead of plane waves can improve the results, but that is a future project.

Let us go back now to the integral (11). The best solution is to calculate the time-dependent Schrödinger equation) (8) numerically, and then the 9D integral (11). This problem has not yet been solved, and we limited ourselves to the model described above with the distorted-wave Born approximation (DWBA) closure approximation. This model has two specific features: (1) it includes no fitting parameters like the averaged energy (the corresponding exponents cancel each other), and (2) the intermediate helium ion stays in its ground state during the fast collision process. The results of the calculations are presented in Figs. 9–11. We see the tendency of the modified PWFBA to move toward the PWFBA results with an increase of energy, but this model of the DWBA with a nonperturbed intermediate ion does not work. Perhaps we can improve the results by considering the 9D integral with the full eikonal (14), but this project is also for the future.

V. CONCLUSIONS

In conclusion, we have presented a systematic study of electron transfer in the most fundamental collision system p-He at rather high impact energies ($E_p = 630$, 1000, and 1200 keV). We have been able to separate the pure transfer process from additional excitation contributions, which account for up to 25% of the total electron-capture cross section. We have considered a few models for the theoretical description of the fast reaction $p + \mathrm{He} \to \mathrm{H}(n = 1) + \mathrm{He}^+(n' = 1)$, namely, the PWFBA, the PWSBA with closure, and the DWBA with closure. At present, the PWSBA model provides the best fit to the experiment but many physical questions remain open.

ACKNOWLEDGMENTS

This work was supported by DFG, the BMBF, and Roentdek GmbH. O.Ch. and Yu.V.P. acknowledge the Russian Foundation for Basic Research (Grant No. 11-01-00523) for financial support. O.Ch. acknowledges financial support from Project No. 09-6-1060-2005/2013, "Mathematical Support of Experimental and Theoretical Studies Conducted by JINR."

[1] M. Gudmundsson, D. Fischer, N. Haag, H. A. B. Johansson, D. Misra, P. Reinhed, H. Schmidt-Böcking, R. Schuch, M. Schöffler, and K. Stochkel, J. Phys. B **43**, 185209 (2010).
[2] R. Shakeshaft and L. Spruch, Rev. Mod. Phys. **51**, 369 (1979).
[3] D. Belkic, I. Mancev, and J. Hanssen, Rev. Mod. Phys. **80**, 249 (2008).
[4] J. R. Oppenheimer, Phys. Rev. **31**, 349 (1928).
[5] H. C. Brinkman and H. A. Kramers, Proc. K. Ned. Akad. Wet. **33**, 973 (1930).
[6] L. H. Thomas, Proc. R. Soc. A **114**, 561 (1927).
[7] E. Horsdal, B. Jensen, and K. O. Nielsen, Phys. Rev. Lett. **57**, 1414 (1986).
[8] E. Horsdal-Pedersen, C. L. Cocke, and M. Stöckli, Phys. Rev. Lett. **50**, 1910 (1983).
[9] D. Fischer, M. Gudmundsson, Z. Berényi, N. Haag, H. A. B. Johansson, D. Misra, P. Reinhed, A. Källberg, A. Simonsson, K. Støchkel, H. Cederquist, and H. T. Schmidt, Phys. Rev. A **81**, 012714 (2010).
[10] D. Fischer, K. Støchkel, H. Cederquist, H. Zettergren, P. Reinhed, R. Schuch, A. Källberg, A. Simonsson, and H. T. Schmidt, Phys. Rev. A **73**, 052713 (2006).
[11] R. Ali, V. Frohne, C. L. Cocke, M. Stockli, S. Cheng, and M. L. A. Raphaelian, Phys. Rev. Lett. **69**, 2491 (1992).
[12] V. Mergel, R. Dörner, J. Ullrich, O. Jagutzki, S. Lencinas, S. Nüttgens, L. Spielberger, M. Unverzagt, C. L. Cocke, R. E. Olson, M. Schulz, U. Buck, E. Zanger, W. Theisinger, M. Isser, S. Geis, and H. Schmidt-Böcking, Phys. Rev. Lett. **74**, 2200 (1995).
[13] D. Fischer, B. Feuerstein, R. D. DuBois, R. Moshammer, J. R. C. Lopez-Urrutia, I. Draganic, H. Lörch, A. N. Perumal, and J. Ullrich, J. Phys. B **35**, 1369 (2002).
[14] J. Ullrich, R. Moshammer, R. Dörner, O. Jagutzki, V. Mergel, H. Schmidt-Böcking, and L. Spielberger, J. Phys. B **30**, 2917 (1997).
[15] R. Dörner, V. Mergel, O. Jagutzki, L. Spielberger, J. Ullrich. R. Moshammer and H. Schmidt-Böcking, Phys. Rep. **330**, 95 (2000).
[16] J. Ullrich, R. Moshammer, A. Dorn, R. Dörner, L. Ph. H. Schmidt, and H. Schmidt-Böcking, Rep. Prog. Phys. **66**, 1463 (2003).
[17] M. S. Schöffler, J. Titze, L. Ph. H. Schmidt, T. Jahnke, N. Neumann, O. Jagutzki, H. Schmidt-Böcking, R. Dörner, and I. Mancev, Phys. Rev. A **79**, 064701 (2009).
[18] O. Jagutzki, J. S. Lapington, L. B. C. Worth, U. Spillman, V. Mergel, and H. Schmidt-Böcking, Nucl. Instrum. Methods Phys. Res., Sect. A **477**, 256 (2002).
[19] O. Jagutzki, V. Mergel, K. Ullmann-Pfleger, L. Spielberger, U. Spillmann, R. Dörner, and H. Schmidt-Böcking, Nucl. Instrum. Methods Phys. Res., Sect. A **477**, 244 (2002).
[20] R. Dörner, V. Mergel, L. Spielberger, M. Achler, Kh. Khayyat, T. Vogt, H. Bräuning, O. Jagutzki, T. Weber, J. Ullrich, R. Moshammer, M. Unverzagt, W. Schmitt, H. Khemliche, M. H. Prior, C. L. Cocke, J. Feagin, R. E. Olson, and H. Schmidt-Böcking, Nucl. Instrum. Methods Phys. Res., Sect. B **124**, 225 (1997).

[21] J. Ullrich, R. E. Olson, R. Dörner, V. Dangendorf, S. Kelbch, H. Berg, and H. Schmidt-Böcking, J. Phys. B **22**, 327 (1989).
[22] S. Houamer, Yu. V. Popov, and C. Dal Cappello, Phys. Rev. A **81**, 032703 (2010).
[23] P. S. Vinitsky, Yu. V. Popov, and O. Chuluunbaatar, Phys. Rev. A **71**, 012706 (2005).
[24] M. Schöffler, Ph.D. thesis, Johann Wolfgang Goethe-Universität, Frankfurt am Main, 2006 [http://publikationen.ub.uni-frankfurt.de/volltexte/2006/3536/].
[25] Dž. Belkić, R. Gayet, and A. Salin, Phys. Rep. **56**, 279 (1979).
[26] E. Weigold and I. E. McCarthy, *Electron Momentum Spectroscopy* (Kluwer, New York, 1999).
[27] V. G. Neudatchin, Yu. V. Popov, and Yu. F. Smirnov, Phys. Usp. **42**, 1017 (1999).
[28] Yu. V. Popov, O. Chuluunbaatar, V. L. Shablov, and K. A. Kouzakov, Phys. Part. Nuclei **41**, 543 (2010).
[29] S. Houamer, Yu. V. Popov, and C. Dal Cappello, Phys. Lett. A **373**, 4447 (2009).